Conditional Deletion of Insulin-like Growth Factor-I Receptor in Prostate Epithelium

Brent W. Sutherland,[1] Sue E. Knoblaugh,[2] Paula J. Kaplan-Lefko,[4] Fen Wang,[5] Martin Holzenberger,[6] and Norman M. Greenberg[1,3]

[1]Clinical Research Division and [2]Animal Health Shared Resources, Fred Hutchinson Cancer Research Center; [3]Department of Pharmacology, University of Washington, Seattle, Washington; [4]Department of Molecular and Cellular Biology, Baylor College of Medicine; [5]Center for Cancer and Stem Cell Biology, Institute of Biosciences and Technology, Texas A&M Health Science Center, Houston, Texas; and [6]Institut National de la Sante et de la Recherche Medicale U515, Saint-Antoine Hospital, Paris, France

Abstract

Insulin-like growth factor-I (IGF-I) is a polypeptide hormone that can influence growth, differentiation, and survival of cells expressing the cognate type 1 receptor (IGF-IR). To better understand cell autonomous IGF-IR signaling in the epithelial compartment of the prostate gland, we generated a conditional (Cre/loxP) prostate-specific IGF-IR knockout mouse model. In contrast to epidemiologic studies that established a correlation between elevated serum IGF-I and the risk of developing prostate cancer, we show that abrogation of IGF-IR expression in the dorsal and lateral prostate could activate extracellular signal-regulated kinase 1/2 signaling and cause cell autonomous proliferation and hyperplasia. Moreover, persistent loss of IGF-IR expression in dorsal and ventral lobes induced p53-regulated apoptosis and cellular senescence rescue programs, predicting that titration of IGF-IR signaling might facilitate growth of tumors with compromised p53 activity. Therefore, we crossed the mice carrying the prostate-specific IGF-IR knockout alleles into the transgenic adenocarcinoma of the mouse prostate model that is driven, in part, by T antigen–mediated functional inactivation of p53. Consistent with our prediction, prostate epithelial–specific deletion of IGF-IR accelerated the emergence of aggressive prostate cancer when p53 activity was compromised. Collectively, these data support a critical role for IGF-IR signaling in prostate tumorigenesis and identify an important IGF-IR–dependent growth control mechanism. [Cancer Res 2008;68(9):3495–504]

Introduction

Prostate cancer remains the most common malignancy diagnosed in men in the United States with mortality second only to lung and bronchus cancers. These statistics underscore the need to elucidate and characterize the molecular mechanisms that predispose and promote spontaneous disease and the development of efficacious targeted therapeutic strategies for prevention and intervention. Because the insulin-like growth factor (IGF) signaling pathway has been implicated by clinical, epidemiologic, and experimental data as a contributing factor in the natural history of prostate cancer, strategies to target the IGF-I axis are being developed. Unfortunately, efforts to thoroughly investigate the causal relationship between IGF-I signaling and prostate cancer or validate the efficacy of anti–IGF-I-based therapies for autochthonous spontaneous disease have been hindered by the complexity of the IGF-I axis, the heterogeneous nature of clinical prostate cancer, and the paucity of appropriate models.

The IGF signaling axis is composed of two highly homologous ligands, IGF-I and IGF-II, and their cognate tyrosine kinase receptor [IGF type I receptor (IGF-IR)]. A structurally distinct second receptor (IGF-IIR) binds and internalizes IGF-II but does not directly contribute to transmembrane signaling. A conserved family of six homologous IGF-binding proteins (IGFBP-1 to IGFBP-6) with high affinity for IGF-I and IGF-II, and two IGFBP-related proteins (IGFBP-rP1 and IGFBP-rP2) have been described (see refs. 1–6 for recent reviews). The circulating IGF-I ligand is mainly synthesized and secreted by the liver under control of growth hormone (GH). Production and pulsatile secretion of GH in the juvenile and adult pituitary gland are regulated by antagonistic actions of hypothalamic GH-releasing hormone (GHRH), somatostatin, and their corresponding receptors. The entire somatotropic neuroendocrine function is modulated by multiple hypothalamic and pituitary responses to such factors as stress, exercise, nutrition, and the hormone ghrelin. IGF-I functions primarily as a polypeptide hormone regulator of growth but is known to exert additional metabolic effects. Although IGF-I is also produced in other tissues and organs such as the prostate, the regulation and consequence of localized IGF-I production remain the subject of investigation.

The IGF-IR transmembrane tyrosine kinase receptor is composed of two extracellular α-subunits that constitute the ligand-binding domain and two intracellular β-subunits that constitute the kinase domain. Ligand-dependent activation of the IGF-IR kinase can initiate multiple signaling events in part through phosphorylation of insulin receptor substrate (IRS) proteins, a family of which IRS-1 is the predominant member. Other notable downstream molecules that can transduce IGF-IR signals include SHC, Grb2, SHP2, phosphatidylinositide-3′-kinase (PI3κ), Akt, and mitogen-activated protein kinase (MAPK; refs. 7–9).

Increased lifetime prostate cancer risk has been associated with levels of serum IGF-I in the high reference range (10). Elevated levels of IGFBP-2 and reduced levels of IGFBP-3 have also been found in serum and prostate tissues of prostate cancer patients. Because IGFBP-3 is a primary carrier of IGF in serum, decreased functional expression of IGFBP-3 could influence the level of bioavailable IGF. This is of particular interest in prostate cancer because prostate-specific antigen, a kallikrein serine protease often found elevated in patients with prostate cancer, can cleave IGFBP-3 (11). In contrast to serum IGF-I, there is limited and conflicting data about the role of IGF-IR in clinical cancers. For example,

Note: Supplementary data for this article are available at Cancer Research Online (http://cancerres.aacrjournals.org/).

Current address for B.W. Sutherland: Biomedical Research Center, University of British Columbia, Vancouver, British Columbia, Canada.

Current address for P.J. Kaplan-Lefko: AMGEN, Thousand Oaks, CA.

Requests for reprints: Norman M. Greenberg, Clinical Research Division, Fred Hutchinson Cancer Research Center, Seattle, WA 98109. Phone: 206-667-4433; Fax: 206-667-4930; E-mail: ngreenberg@fhcrc.org.

doi:10.1158/0008-5472.CAN-07-6531

enforced expression of IGF-IR can cause fibroblasts to display a malignant phenotype in xenografts (12), whereas blockade of IGF-IR cellular activity impeded neoplastic progression in other model systems (see refs. 1, 13 for recent reviews). Reduced levels of both IGF-I and IGF-IR have been noted in disseminated androgen depletion-independent specimens from human (14) and mouse (15) prostate cancer, whereas elevated levels of IGF-IR have been correlated with reduced metastasis, local recurrence, and disease-free survival for patients with malignant soft tissue sarcomas (16). Recent reports have also shown that selective suppression of the IGF-IR signaling substrate IRS-1, favoring the function of IRS-2, can promote metastatic breast cancer in transgenic mice (17).

An emerging paradox from clinical and experimental studies is that IGF action can help cells survive transformation while simultaneously imposing a strong differentiation signal that may slow tumor progression. We have recently shown that enforced IGF-I signals can cause spontaneous preneoplastic changes in the prostate in a genetically engineered mouse (GEM) model and that selection against this same signal was concomitant with the emergence of more aggressive metastatic states (18), consistent with clinical data (14). Based on these findings, we proposed the "hurdle hypothesis" to explain how the strength of the IGF-I signal can help define the height of a differentiation hurdle that in turn determines how aggressive a cancer must become to achieve malignancy (18).

The role of the IGF-I axis in prostate cancer has been investigated in other GEM models with mixed results relative to clinical observations. In one system, expression of human IGF-I in basal epithelia under control of a bovine keratin 5 promoter (BK5-IGF-I) coordinately elevated systemic levels of IGF-I and IGFBP-3 (19, 20). These BK5-IGF-I mice developed hyperplasia, prostatic intraepithelial neoplasia (PIN) lesions, and prostatic adenocarcinoma, as well as skin cancer and many other anomalies. Although elevated IGF-I and IGFBP-3 are often observed in the serum of acromegalics (21), the patients do not seem specifically predisposed to prostate cancer. Hence, the tumors observed in the BK5-IGF-I mice may actually represent the consequence of the simultaneous activation of a variety of signaling programs in multiple tissue compartments. In another model, enforced systemic expression of rat prolactin under transcriptional control of the metallothionein promoter caused elevated serum levels of prolactin, IGF-I, and testosterone. Although these mice developed enlarged and hyperplastic prostate glands, they did not develop tumors (22, 23). Taken together, the data from GEM models show that the context in which IGF-I signaling is activated seems to be a major determinant of the resulting phenotype.

Using a model of multistage prostate tumorigenesis based on tissue-restricted abrogation of the p53 and Rb tumor suppressor pathways (24), we have previously shown that the prostate can actually be a source of IGF-I expression (15). In the transgenic adenocarcinoma of the mouse prostate (TRAMP) model, serum IGF-I was found to be precociously elevated during prostate cancer progression and serum levels of IGFBP-2 correlated with advanced prostate cancer, in keeping with reports from clinical disease (25, 26). Whereas expression of IGF-IR mRNA was found to increase in the prostate during tumor development in TRAMP, expression was dramatically reduced in metastatic lesions arising in the intact and castrated mice. Using the TRAMP system, we have also shown that a germ-line mutation that disrupts GHRH receptor signaling to reduce circulating levels of both GH and IGF-I (the *lit* mutation; ref. 27) could slow the initiation and progression of primary prostate cancer (28).

In this report, we describe a conditional prostate-specific IGF-IR knockout model to directly investigate how IGF-IR signaling *in vivo* can influence cellular homeostasis and cancer. Although we expected that selective abrogation of IGF-IR in prostate epithelium would cause widespread cell death and resistance to oncogene-mediated transformation (29), we actually observed a lobe-specific proliferative response in terminally differentiated prostate epithelium and the emergence of prostatic hyperplasia in young mice. In aged mice, we observed that IGF-IR deletion-dependent apoptosis and cellular senescence responses both coincided with the accumulation of stabilized p53, whereas expression of p21 and plasminogen activator inhibitor-1 (PAI-1) specifically correlated with cellular senescence. Although these findings support a critical role for the IGF axis in maintaining tissue homeostasis and differentiation, they also suggest that therapeutics targeting the IGF-I signaling axis might facilitate growth of tumor cells when p53 activity is compromised. To directly test this possibility, we created compound GEM models crossing the conditional IGF-IR alleles into the TRAMP model and showed that conditional deletion of the IGF-IR actually promoted an earlier emergence of more aggressive localized disease. These findings support a very cautious translation of IGF titration strategies to the bedside.

Materials and Methods

Strains and breeding. All animal studies were conducted in accordance with institutional guidelines for humane animal treatment. Mice were maintained at 22°C in a 12-h light and dark cycle with *ad libitum* access to water and food. Mice hemizygous for the ARR2PBi-Cre mice transgene (30) were maintained in a pure FVB/NJ background. The loxP-tagged IGF-IR mice (31) were maintained homozygous (IGF-IR$^{loxP/loxP}$) in a pure 129/SvJ background. TRAMP mice were maintained hemizygous for the PB-Tag transgene in a pure C57BL/6 background. As required, [IGF-IR$^{loxP/wt}$;ARR2PBi-Cre] F1 animals (50% 129; 50% FVB) were crossed to [IGF-IR$^{loxP/wt}$;TRAMP] F1 animals (50% 129; 50% B6) to generate all the mice (25% FVB; 50% 129; 25% B6) for the study.

Genotyping. Isolation of tail DNA and *ex vivo*–harvested tissue DNA for PCR-based screening assays were performed as previously described (24, 32). Alternatively, 5-μm paraffin sections on slides were deparaffinized by standard ethanol/xylene protocols. DNA was extracted from individual prostate lobes using the PicoPure DNA Extraction kit (Arcturus Bioscience) according to the manufacturer's instructions. Identification of ARR2PBi-Cre transgenic mice used primers CF (5′-ATCTGGCATTTCTGGGGATTG-3′) and CR (5′-CTACACCAGAGACGGAAATCCATC-3′) to yield a 256-bp fragment. Identification of PB-Tag mice used primers Pb-1 forward (5′-CCGGTCGACCGGAAGCTTCCACAAGTGCATTTA-3′) and SV40TagRev (5′-CTCCTTTCAAGACCTAGAAGGTCCA-3′) to amplify a 650-bp fragment. Identification of the wild-type (wt) or loxP-modified IGF-IR loci used primers RLmt (5′-ATCTTGGAGTGGTGGGTCTGTTTC-3′) and RLvt (5′-ATGAATGCTGGTGAGGGTTGTCTT-3′) to amplify 312-bp loxP IGF-IR and 256-bp wt IGF-IR fragments. Deletion of IGF-IR exon 3 was confirmed using primers RLvt and RLex (5′-CCATGGGTGTTAAATGTAATGGC-3′), yielding a 204-bp fragment.

Histology. At necropsy, the entire genitourinary tract consisting of the bladder, urethra, seminal vesicles, ampullary gland, and the prostate was excised, weighed, and dissected under a microscope. The dorsal (DP), lateral (LP), ventral (VP), and anterior (AP) prostate lobes were separated when possible. Tissues were fixed in 4% paraformaldehyde for 36 to 48 h at 4°C and processed into paraffin blocks. Multiple 5-μm sections were cut and stained with H&E. Histopathology was determined according to the GEM grading classification scheme (33) and expressed as the percentage of total gland area exhibiting murine PIN (with or without nuclear atypia), well differentiated adenocarcinoma, moderately differentiated adenocarcinoma, poorly differentiated adenocarcinoma, or carcinoma with a phylloides-like appearance.

Immunohistochemistry. The 5-μm paraffin sections were deparaffinized by standard ethanol/xylene protocols and sequentially placed in boiling 10 mmol/L citric acid for 30 min for antigen retrieval, 3% hydrogen

peroxidase/methanol to block endogenous peroxidase activity, and SuperBlock (Pierce Scientific) for 1 h at room temperature. Primary antibodies and working dilutions were as follows: anti-Cre recombinase (1:1,000; Novagen), anti-IGF-IRα (1:200; Santa Cruz Biotechnology), anti-E-cadherin (1:750; BD Biosciences), anti-p63 (1:1,000; NeoMarkers), anti-smooth muscle actin (SMA; 1:500; Sigma), anti-Ki67 antibody (1:1,000; Novocastra Laboratories), anti-active caspase-3 (1:100; Fisher), anti-phosphorylated p44/42 (1:200; Cell Signaling), or anti-p44/42 (1:200, Cell Signaling). All antibodies were diluted in SuperBlock and samples were incubated overnight at 4°C with gentle rocking. Primary antibodies were detected with biotinylated anti-rabbit IgG (H+L; 1:100; Vector) or the DakoCytomation LSAB+System-HPR universal detection system with 3,3′-diaminobenzidine substrate. Slides were counterstained with 0.1% methyl green or a mild hematoxylin treatment.

Proliferation rate. Analysis with an anti-Ki67 antibody identified proliferating cells. Three to six random fields were counted at ×400 magnification to obtain the proliferation index. Averages (±SD) were calculated from data obtained from three mice per cohort and significance was determined using the two-sided, two-tailed Student's *t* test method.

Cell death. Apoptotic cells were identified by terminal deoxynucleotidyl transferase–mediated dUTP nick end labeling (TUNEL) assay according to the manufacturer's instructions (In Situ Cell Death Detection Kit-AP, Boehringer Mannheim). Because TUNEL staining recognizes fragmented DNA, we confirmed that cells were undergoing apoptosis by assessing abnormal nuclear morphology and by using an antibody to detect active caspase-3 (as described above). The relative amount of TUNEL staining was determined using The NIH ImageJ software analysis package. At least six random fields of view (×400 magnification) were used to calculate the average pixel intensity. Significance was determined using the two-sided Student's *t* test method.

Western blot analysis. Total protein lysates were prepared from prostate tissues by homogenization in 50 mmol/L Tris (pH 8), 150 mmol/L NaCl, 5 μg/mL leupeptin, 5 μg/mL pepstatin, 1 mmol/L phenylmethylsulfonyl fluoride, 1 mmol/L sodium orthovanadate, 10 mmol/L NaF, and 1% Triton X-100. Approximately 40 to 50 μg of protein from each sample were denatured in lithium dodecyl sulfate loading buffer (Invitrogen) by boiling for 10 min and loaded onto 8% or 10% SDS-polyacrylamide gels. Proteins separated by electrophoresis were transferred to Immobilon-P nylon membranes (Millipore) and filters were blocked for 1 to 2 h at room temperature in PBS-Tween (0.1%, v/v) and 5% (w/v) nonfat dry milk (Carnation). Primary antibodies (and working dilutions) were as follows: anti-IGF-IRα (1:750), anti-phosphorylated IGF-IR/IR (1:1,000; Cell Signaling), anti-phosphorylated p44/42 (1:1,000), anti-p44/42 (1:1,000), anti-phosphorylated Akt (1:1,000; Cell Signaling), anti-Akt (1:1,000; Cell Signaling), anti-phosphorylated Src (1:1,000; Cell Signaling), anti-phosphorylated A-Raf (1:1,000; Cell Signaling), anti-phosphorylated C-Raf (1:1,000; Cell Signaling), anti-phosphorylated MAPK/extracellular signal-regulated kinase (ERK) kinase (MEK) 1/2 (1:1,000; Cell Signaling), anti-E-cadherin (1:2,000), anti-protein phosphatase 2A (PP2A; 1:500; Santa Cruz Biotechnology), anti-MAPK phosphatase 3 (MKP3; 1:500; Santa Cruz Biotechnology), anti-p53 (1:1,000; Santa Cruz Biotechnology), anti-p21 (1:500; Santa Cruz Biotechnology), anti-PAI-1 (1:1,000; Santa Cruz Biotechnology), anti-androgen receptor (AR; 1:2,000; Upstate), or anti-mouse probasin (1:3,000; in-house rabbit polyclonal; ref. 34) diluted in 5% bovine serum albumin in PBS-Tween (0.1%, v/v) and incubated at 4°C overnight with gentle rocking. Membranes were washed thrice for 5 min with PBS-Tween (0.1%, v/v) and incubated with either horseradish peroxidase–conjugated anti-rabbit or anti-mouse (Bio-Rad) IgG antibody diluted 1:20,000 or 1:5,000, respectively, for 1.5 h at room temperature in 5% nonfat dry milk in PBS-Tween (0.1%, v/v). Membranes were washed thrice for 5 min with PBS-Tween and routinely developed using either enhanced chemiluminescence Western blotting detection system (Amersham Biosciences) or SuperSignal West Femto Maximum Sensitivity Substrate (1:5 dilution in water; Pierce Scientific) and exposed to X-ray film (XAR-1, Eastman Kodak). The NIH ImageJ software analysis package was used to determine the level of IGF-IR protein. Background and sample loading variation were determined from negative controls and β-actin intensities, respectively.

Results

Conditional deletion of IGF-IR causes hyperplasia and proliferation. To study the role of IGF-IR in prostate epithelium *in vivo*, we crossed the transgenic ARR2PBi-Cre activator mice (30) to mice harboring IGF-IR loxP-tagged genomic loci (31) generating the IGF-IR$^{loxP/loxP}$;ARR2PBi-Cre (IGF-IR knockout), IGF-IR$^{loxP/wt}$;ARR2PBi-Cre (IGF-IR titrated), and littermate [IGF-IR$^{loxP/loxP}$ or IGF-IR$^{loxP/wt}$] controls (IGF-IR intact). Hereafter, the presence of ARR2PBi-Cre will simply be denoted as "Cre".

The consequence of prostate epithelial–specific abrogation of IGF-IR was examined in adult bigenic IGF-IR$^{loxP/loxP}$;Cre (n = 10), IGF-IR$^{loxP/wt}$;Cre (n = 12), and control IGF-IR$^{loxP/loxP}$ or IGF-IR$^{loxP/wt}$ (n = 10) mice at 12 weeks of age. As shown in Table 1, we observed no significant changes in animal weight, genitourinary tract (consisting of bladder, prostate glands, seminal vesicles, urethra, and ampullary gland) weight, the genitourinary/animal weight ratio, or prostate lobe wet weights between the various groups. Prostate-restricted knockout of IGF-IR did not influence overall body weight or prostate mass. Male IGF-IR$^{loxP/loxP}$;Cre mice remained fertile up to 37 weeks of age (data not shown).

As shown in Fig. 1, expression and localization of Cre protein were restricted to the luminal prostate epithelial cells of mice harboring the Cre transgene consistent with findings from previous studies (34–36). To date, no developmental defects associated with ARR2-Pbi-Cre expression have been reported. Similarly, we were unable to detect any prostate developmental defects associated with Cre expression at 6 weeks in IGF-IR$^{loxP/wt}$;Cre mice (data not shown).

The extent of prostate tissue–specific recombination at the IGF-IR loci was determined from DNA of multiple tissues of

Table 1. Consequence of IGF-IR titration and ablation on the prostate

Genotype	Age (wk)	*n*	Animal weight (g)*	Genitourinary average (mg)	Genitourinary/animal (g)	Prostate weight (mg)	Prostate/animal (mg/g)	Seminal vesicle weight (mg)
IGF-IR$^{loxP/loxP\ or\ loxP/wt}$	12	10	32.4 ± 3.4	360 ± 90	0.011 ± 0.002	40 ± 11	1.2 ± 0.3	178 ± 48
	24	14	36.5 ± 5.2	480 ± 150	0.013 ± 0.003	56 ± 10	1.6 ± 0.3	243 ± 62
IGF-IR$^{loxP/wt}$;Cre	12	12	32.3 ± 3.9	370 ± 80	0.011 ± 0.003	38 ± 10	1.1 ± 0.3	179 ± 39
	24	12	36.6 ± 4.3	470 ± 80	0.013 ± 0.002	51 ± 9	1.3 ± 0.3	274 ± 62
IGF-IR$^{loxP/loxP}$;Cre	12	10	32.7 ± 3.5	350 ± 60	0.011 ± 0.002	42 ± 10	1.3 ± 0.3	170 ± 44
	24	15	36.8 ± 4.1	450 ± 70	0.012 ± 0.003	51 ± 8	1.4 ± 0.2	244 ± 68

*Mean ± SE.

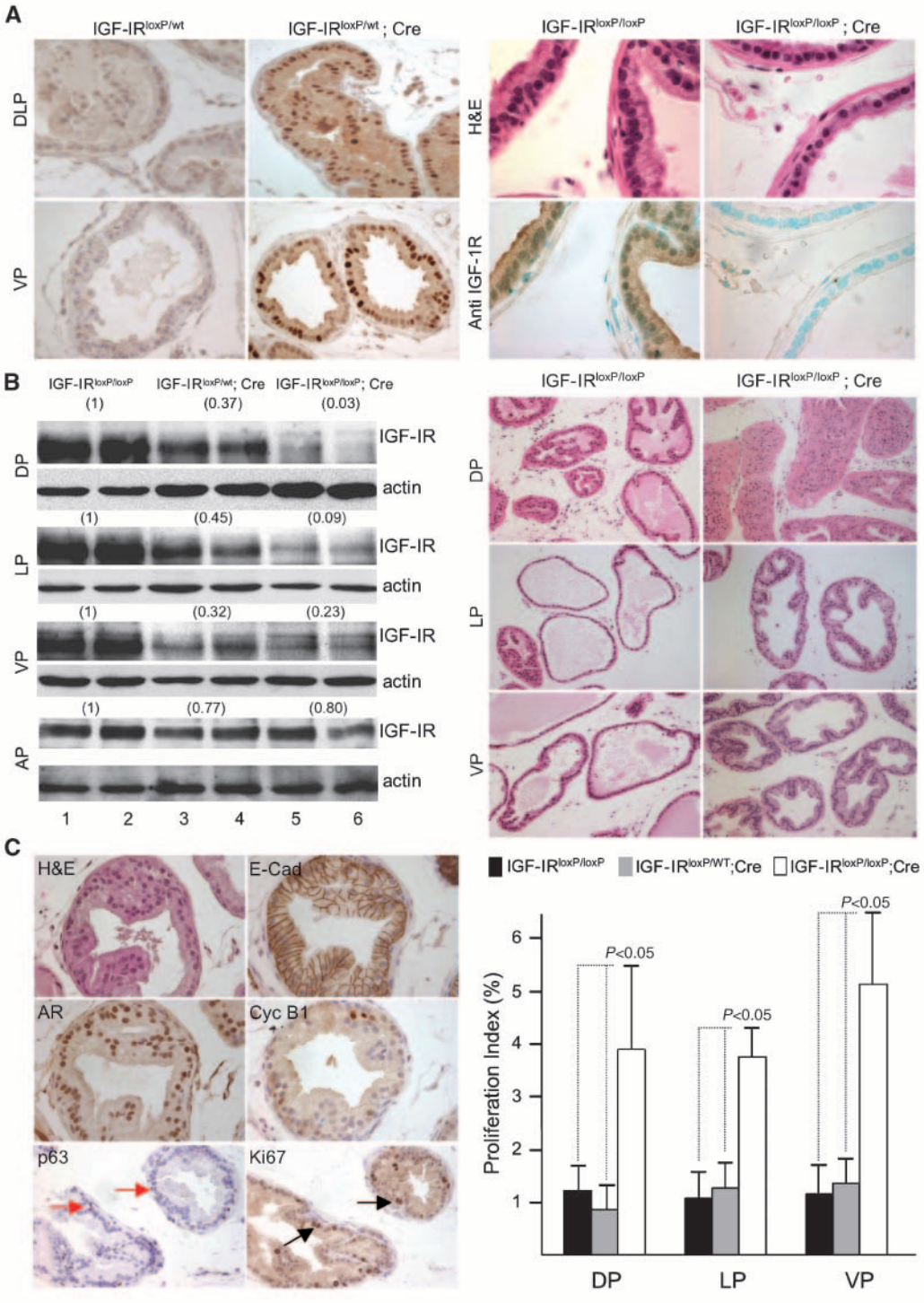

Figure 1. Conditional deletion of IGF-IR in prostate epithelial cells causes proliferation. *A, left,* immunohistochemical analysis with anti-Cre antibody to show how expression of transgene-encoded Cre recombinase (*brown nuclei*) is restricted to epithelium of prostate glands in DLP (*top*) and VP (*bottom*) tissues in IGF-IR$^{loxP/wt}$;Cre at 6 wk of age. No Cre expression was detected in IGF-IR$^{loxP/wt}$ mice. Magnification, ×200. *Right,* IGF-IR is expressed in IGF-IR$^{loxP/loxP}$ mice but absent in IGF-IR$^{loxP/wt}$;Cre mice by 12 wk of age. Nuclei were counterstained with methyl green. Magnification, ×400. *B, left,* immunoblot analysis to show IGF-IR expression in all lobes of IGF-IR$^{loxP/loxP}$ mice (*lanes 1* and *2*), Cre-specific titration of IGF-IR protein in DP, LP, and VP lobes of IGF-IR$^{loxP/wt}$;Cre (*lanes 3* and *4*), and abrogation of IGF-IR protein in IGF-IR$^{loxP/loxP}$;Cre (*lanes 5* and *6*) mice. Expression of β-actin verified equal loading. The levels of IGF-IR protein (relative to control; *lanes 1* and *2*) are indicated in brackets. *Right,* representative formalin-fixed and paraffin-embedded sections from IGF-IR$^{loxP/loxP}$ and IGF-IR$^{loxP/loxP}$;Cre mice stained with H&E to show Cre-dependent expansion of epithelium compartment consistent with proliferative response. Magnification, ×200. *C, left,* robust expression of E-cadherin (*E-Cad*), AR, and cyclin B1 (*Cyc B1*) in DLP of 12-wk-old IGF-IR$^{loxP/loxP}$;Cre mice by immunohistochemistry. Analysis with anti-Ki67 and anti-p63 antibodies shows the proliferative response is restricted to the epithelial and not basal compartment. Magnification, ×400. *Right,* proliferation index calculated from percentage (%) of Ki67-positive cells in prostate lobes of IGF-IR$^{loxP/loxP}$, IGF-IR$^{loxP/wt}$;Cre, and IGF-IR$^{loxP/loxP}$;Cre mice at 12 wk of age. *Columns,* average; *bars,* SD. *P* value was calculated using two-sided Student's *t* test at 95% confidence.

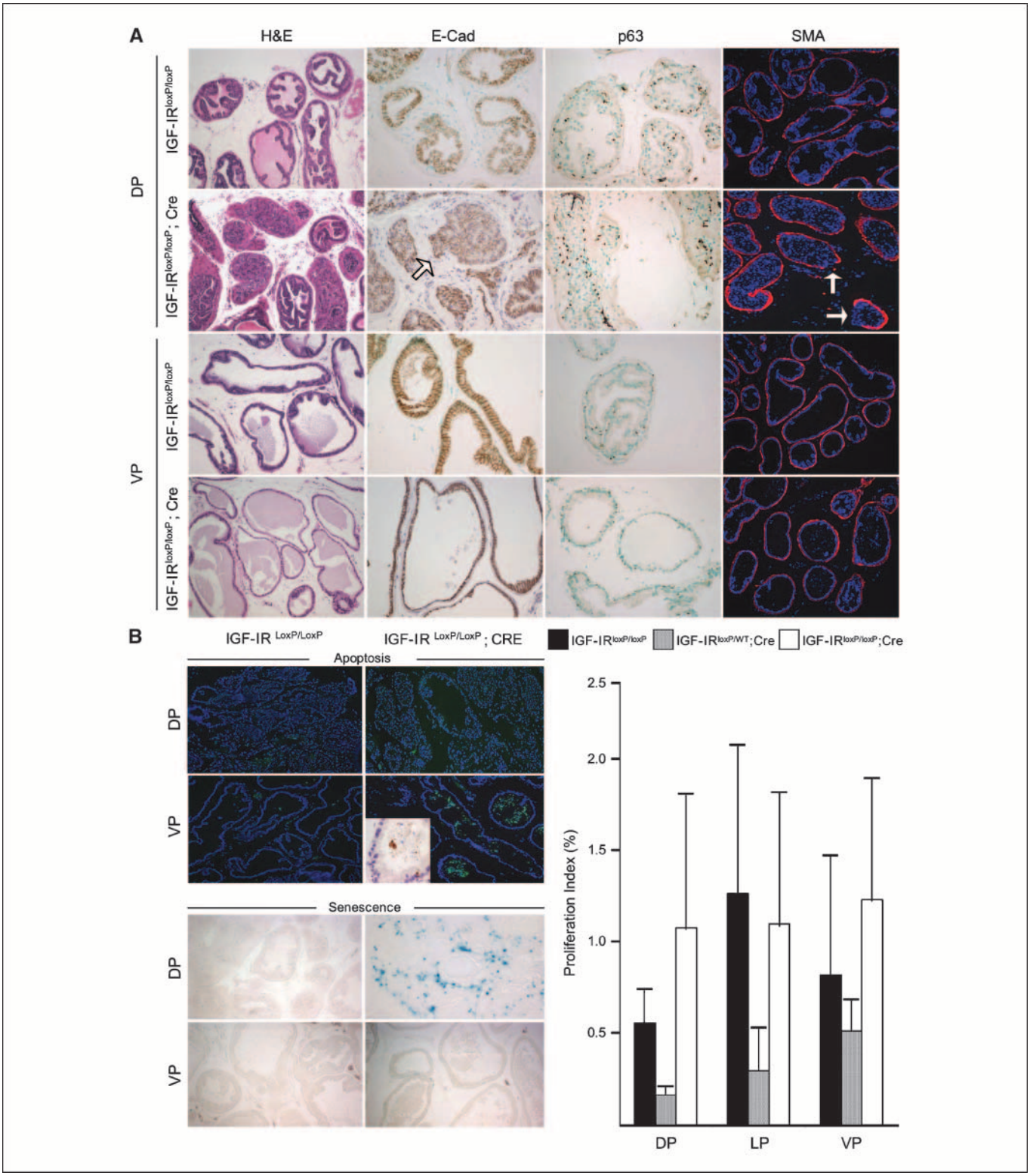

Figure 2. Abrogated IGF-IR expression in the prostate causes minimally invasive disease with lobe-specific apoptosis or senescence. *A,* representative formalin-fixed and paraffin-embedded sections of DP and VP from IGF-IR$^{loxP/loxP}$ and IGF-IR$^{loxP/loxP}$;Cre mice at 24 wk of age were stained with H&E or analyzed by immunohistochemistry with antibodies to E-cadherin, p63, and SMA. Nuclei were counterstained with methyl green or 4′,6-diamidino-2-phenylindole (DAPI; *blue*). *Arrows,* invasion of epithelial cells into surrounding mesenchyme of DP. Original magnification, ×100 (H&E and SMA) or ×200 (E-cadherin and p63). *B, left,* apoptotic cells in VP of IGF-IR$^{loxP/loxP}$;Cre and IGF-IR$^{loxP/loxP}$ mice at 24 wk of age detected by TUNEL. Nuclei were counterstained with DAPI or hematoxylin. Merged images show atypical nuclear morphology associated with apoptosis. *Inset,* apoptotic cells were confirmed by immunostaining for active caspase-3. Original magnifications, ×100 or ×200 (TUNEL; *left* and *right*, respectively) and ×630 (caspase-3). *Bottom,* senescent cells in DP and VP were identified using a β-galactosidase assay on tissues harvested from IGF-IR$^{loxP/loxP}$;Cre and IGF-IR$^{loxP/loxP}$ mice at 24 wk of age. Original magnification, ×200. *Right,* proliferation index in the prostates of IGF-IR$^{loxP/loxP}$, IGF-IR$^{loxP/wt}$;Cre, and IGF-IR$^{loxP/loxP}$;Cre at 24 wk of age determined from the percentage (%) of Ki67-positive epithelial cells in at least three 400× random fields of view. *Columns,* average; *bars,* SD. No significant differences were evident using two-sided Student's *t* test at 95% confidence.

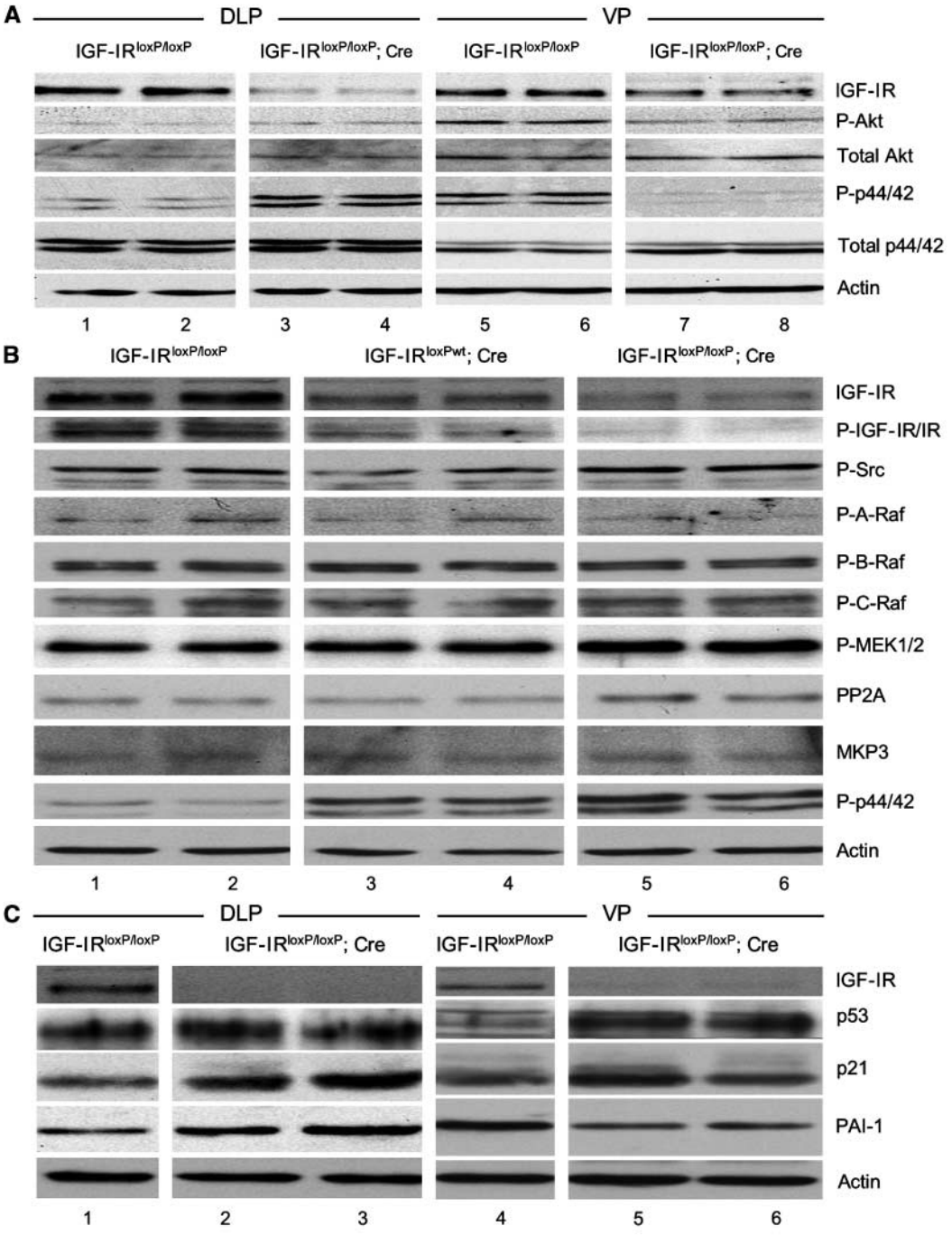

Figure 3. Abrogated expression of IGF-IR deletion causes lobe-specific changes in key downstream signaling targets. *A,* immunoblot analysis of IGF-IR, Akt, and p44/42 expression and activation in DLP (*lanes 1–4*) and VP (*lanes 5–8*) from IGF-IR$^{loxP/loxP}$ (*lanes 1, 2, 5*, and *6*) and IGF-IR$^{loxP/loxP}$;Cre (*lanes 3, 4, 7*, and *8*) mice at 12 wk of age. *B,* immunoblot analysis of IGF-IR, Src, Raf, PP2A, MKP3, and ERK expression and activation in DP from IGF-IR$^{loxP/loxP}$ (*lanes 1* and *2*), IGF-IR$^{loxP/wt}$;Cre (*lanes 3* and *4*), and IGF-IR$^{loxP/loxP}$;Cre (*lanes 5* and *6*) mice at 12 wk of age. *C,* immunoblot analysis of IGF-IR, p53, p21, and PAI-1 expression and activation in DP (*lanes 1–3*) and VP (*lanes 4–6*) samples procured from IGF-IR$^{loxP/loxP}$ (*lanes 1* and *4*) and IGF-IR$^{loxP/loxP}$;Cre (*lanes 2, 3, 5*, and *6*) mice at 24 wk of age. Expression of β-actin was used to verify equal protein loading.

IGF-IR$^{loxP/wt}$;Cre and IGF-IR$^{loxP/loxP}$;Cre mice (Supplementary Fig. S1). At 12 weeks of age, membrane-localized IGF-IR protein was reproducibly detected in VP of IGF-IR$^{loxP/loxP}$ but was dramatically absent in IGF-IR$^{loxP/loxP}$;Cre knockout mice (Fig. 1*A*). A reproducible correlation was also observed between IGF-IR gene dose and level of IGF-IR protein in VP, dorsolateral prostate (DLP), and LP tissues (Fig. 1*B*). There was no apparent compensatory change in expression of the wt IGF-IR allele in IGF-IR$^{loxP/loxP}$;Cre mice consistent with previous reports (31).

Loss of functional IGF-IR caused reproducible gross histologic and epithelial cell–specific changes in the prostates of IGF-IR$^{loxP/loxP}$;Cre mice. As shown in Fig. 1*B*, we observed atypical epithelial tufting,

cribriform structures, epithelial cell layering (epithelial cell hyperplasia), and sheets of cells accumulating within the luminal spaces of the LP and VP. The DP also displayed a disorganized epithelial cell compartment where the morphologically abnormal enlarged and possibly vacuolated epithelial cells (hyperplasia and hypertrophy) were associated with an unusually disorganized luminal space.

The increase in the area of abnormal ductal epithelium was significant between 12-week-old IGF-IR$^{loxP/loxP}$ control mice (n = 7; DP: 13.6 ± 22.5%; LP: 13.8 ± 16.2%; VP: 12.9 ± 9.1%) and 12-week-old IGF-IR$^{loxP/loxP}$;Cre mice (n = 7; DP: 42.5 ± 28.1%; LP: 53.3 ± 39.1%; VP: 63.8 ± 38.5%; Student's t test: $P < 0.05$, DP and LP; $P < 0.005$, VP). The IGF-IR$^{loxP/wt}$;Cre mice displayed an intermediate phenotype compared with controls (n = 10; DP: 24.6 ± 18.9%; LP: 57.0 ± 32.0%; VP: 32.5 ± 21.2%; Student's t test: $P = 0.01$, LP; $P = 0.047$, VP), indicating a dose-response relationship with functional IGF-IR expression.

Loss of functional IGF-IR caused reproducible and significant increase in the proliferation index in all prostate lobes of IGF-IR$^{loxP/loxP}$;Cre (n = 3) mice compared with IGF-IR$^{loxP/loxP}$ (n = 3) and IGF-IR$^{loxP/wt}$;Cre (n = 3) mice (two-sided Student's t test at 95% confidence: $P < 0.05$, DP and VP; $P < 0.01$, LP and AP; Fig. 1*C*). Overall, the levels of Ki67 detected in IGF-IR$^{loxP/wt}$;Cre mice were not significantly different from IGF-IR$^{loxP/loxP}$ mice, suggesting that the proliferative response was not a consequence of IGF-IR haploinsufficiency. Proliferating cells were most frequently localized to atypical and cribriform structures and expressed the luminal marker E-cadherin but not the basal cell marker p63 (Fig. 1*C*). Although there was no appreciable change in steady-state levels of AR with the loss of IGF-IR, there was a decrease in probasin expression (Supplementary Fig. S2) consistent with a change in terminal differentiation status and epithelial function.

Conditional deletion of IGF-IR causes age-dependent apoptosis and senescence. Remarkably, the focal regions of hyperplasia evident at 12 weeks of age did not progress to carcinoma over time. Although IGF-IR$^{loxP/loxP}$;Cre mice displayed significant pathology in DP at 24 weeks (Fig. 2), the integrity of this compartment remained mostly intact based on pattern of p63 and SMA expression, although there was evidence of local invasion in the DP (Fig. 2*A*). Here, the expression of E-cadherin was punctuate and nonuniform and the incidence of abnormal epithelium remained significantly higher relative to that of age-matched control IGF-IR$^{loxP/loxP}$ mice [50.7 ± 9.0% (n = 14) and 16.9 ± 16.2% (n = 17), respectively; $P < 0.0001$, Student's t test]. We were unable to detect significant pathology or evidence of invasive disease in the VP and LP lobes.

Because oncogene-induced proliferation can cause cellular apoptosis or senescence (37), we performed TUNEL analysis and observed a significantly higher apoptotic response restricted to the VP of IGF-IR$^{loxP/loxP}$;Cre mice (Fig. 2*B*) relative to IGF-IR$^{loxP/loxP}$ mice ($P = 0.007$, two-sided Student's t test at 95% confidence). Analysis with an anti-active caspase-3 antibody confirmed the apoptotic response in the epithelial cell compartment (Fig. 2). Using an antibody specific to senescence-associated β-galactosidase (SA-βgal), we also observed the senescence response in DP tissues of IGF-IR$^{loxP/loxP}$;Cre mice relative to controls (Fig. 2*B*). Consistent with an accumulation of lysosomal content, the SA-βgal signal localized to the cytoplasm in discrete pockets. In general, these data support a lobe-specific "switch" in response to abrogated IGF-IR signaling. Our inability to show apoptosis or senescence in LP tissues may indicate that a nonclassic form of cell cycle arrest is induced in these epithelial cells following IGF-IR ablation.

The proliferation index for IGF-IR$^{loxP/loxP}$;Cre mice at 24 weeks was not significantly different than in age- and lobe-matched IGF-IR$^{loxP/loxP}$ and IGF-IR$^{loxP/wt}$;Cre mice (Fig. 2*B*). Given our observations that (*a*) the epithelial cells in the VP were increasingly apoptotic and (*b*) there was increased evidence of senescing cells in the DP phenotype at 12 weeks of age, the abrogation of IGF-IR seemed to have triggered a somewhat self-limiting cellular response.

Conditional deletion of IGF-IR can increase ERK1/2 activation in DP and LP. Following ligand binding, the intracellular activation of IGF-IR β-subunit kinase domain can initiate signaling through the PI3κ/Akt and Ras/MAPK cascades (7–9). As expected, levels of phosphorylated Akt and phosphorylated p44/42 (ERK1/2) levels were consistently reduced in VP of IGF-IR$^{loxP/loxP}$;Cre mice relative to controls (Fig. 3). Surprisingly, in contrast, the steady-state levels of phosphorylated ERK1/2 in DP and LP were increased at 12 weeks of age relative to controls. Moreover, the increased levels of phosphorylated ERK1/2 in DP and LP did not correspond to appreciable changes in phosphorylated Akt levels or phosphorylation of Src kinase, A-Raf, B-Raf, or C-Raf that are known to directly or indirectly activate MEK1/2. Similarly, we were unable to detect changes in steady-state levels of the PP2A

Table 2. Consequence of IGF-IR titration and ablation on prostate cancer

Genotype	Age (wk)	n	Genitourinary range		Genitourinary average (g)*	Genitourinary/ animal (g)	Macroscopic lesion (%) †	Advanced tumors (%) ‡
			Min (g)	Max (g)				
IGF-IR$^{loxP/loxP}$ or IGF-IR$^{loxP/wt}$;TRAMP	18	18	0.31	1.16	0.65 ± 0.20	0.020 ± 0.006	1/18 (6)	2/16 (13)
	24	20	0.43	12.5	2.7 ± 3.35	0.065 ± 0.079	10/20 (50)	7/17 (41)
IGF-IR$^{loxP/wt}$;Cre;TRAMP	18	8	0.41	5.0	1.69 ± 1.57§	0.046 ± 0.047	3/8 (38)	3/7 (43)
	24	6	0.69	1.92	1.18 ± 0.39	0.032 ± 0.011	2/24 (33)	4/6 (67)
IGF-IR$^{loxP/loxP}$;Cre;TRAMP	18	7	0.44	10.5	1.99 ± 3.47	0.050 ± 0.08	1/18 (14)	2/18 (29)
	24	7	0.61	8.68	2.2 ± 2.74	0.052 ± 0.065	6/24 (86)	5/24 (71)

*Mean ± SE.

† Compound tumors (defined as those where the individual lobes were indistinguishable) and lobe confined tumors grossly visible at necropsy.

‡ Poorly differentiated primary carcinomas with no glandular features.

§Significantly increased ($P = 0.02$, two-sided Student's t test at 95% confidence) compared with IGF-IR$^{loxP/loxP}$ or IGF-IR$^{loxP/wt}$;TRAMP at 18 wk of age.

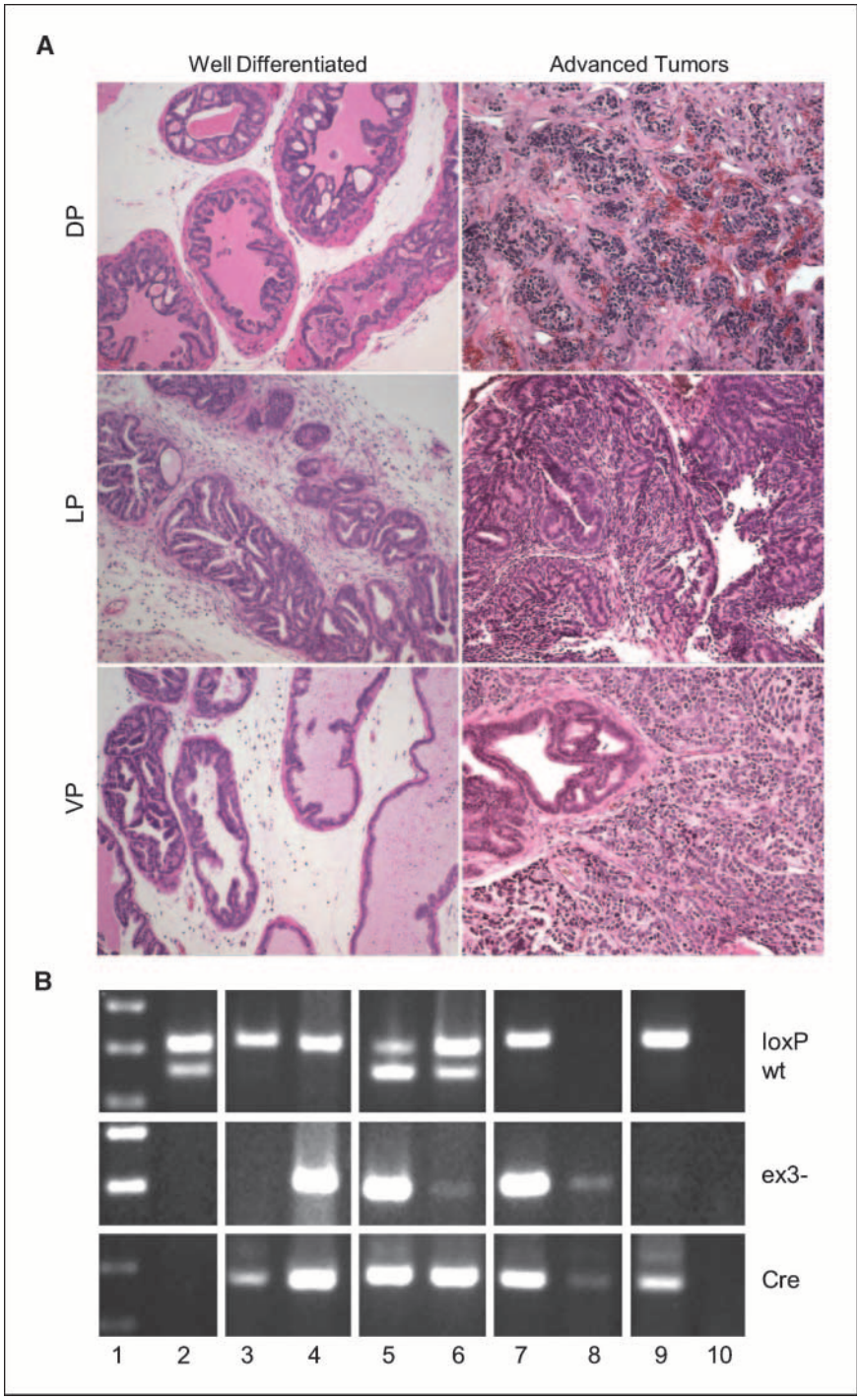

Figure 4. Abrogation of IGF-IR does not prevent or slow progression of spontaneous prostate cancer. *A,* representative sections of well-differentiated and advanced poorly differentiated cancers procured from DP, LP, and VP of IGF-IR$^{loxP/loxP}$;Cre;Tag mice at 24 wk of age stained with H&E. Original magnification, ×100. *B,* PCR analysis was used to detect amplicons from wt (256 bp), loxP-tagged (312 bp), and loxP-recombined (*ex3-*; 204 bp) IGF-IR genomic loci from IGF-IR$^{loxP/loxP}$;Cre;Tag and IGF-IR$^{loxP/wt}$;Cre;Tag mice. *Lane 1,* molecular weight marker; *lane 2,* tail DNA from IGF-IR$^{loxP/wt}$ mouse; *lane 3,* tail DNA; *lane 4,* compound tumor (corresponding to DP in *A*); *lane 5,* intact prostate; *lane 6,* compound tumor (corresponding to tissue in LP in *A*); *lane 7,* intact prostate; *lane 8,* confined phylloides-like tumor (corresponding to advanced VP tumor in *A*); *lane 9,* tail DNA from IGF-IR$^{loxP/loxP}$;Cre;Tag mouse; *lane 10,* water as a control.

and MKP3 phosphatases that negatively regulate both MEK and p44/42. These data clearly show that IGF-IR depletion-dependent activation of p44/42 likely occurs through a nonclassic and as of yet uncharacterized signaling mechanism.

Role of p53 following conditional IGF-IR knockout. The activation, stabilization, and accumulation of the *p53* tumor suppressor gene can induce apoptosis, cell cycle arrest, or cellular senescence in response to cellular stress and declining p53 function has been recently associated with increased tumor incidence as a function of aging (38). To explore the possibility that differential activation of p53-dependent signaling cascades was responsible for the VP-specific apoptosis and DP-specific senescence observed following IGF-IR loss, we examined the steady-state levels of p53 in DP and VP tissues harvested from 12- or 24-week-old IGF-IR$^{loxP/loxP}$;Cre and IGF-IR$^{loxP/loxP}$ mice. Although we did not detect appreciable levels of p53 in any prostate lobe at 12 weeks of age (data not shown), increased steady-state levels of p53 were readily observed in DP and VP from IGF-IR$^{loxP/loxP}$;Cre mice by 24 weeks of age (Fig. 3). These data support a p53-dependent cell-specific link between loss of IGF-IR and the repression of phosphorylated Akt and phosphorylated p44/42 in the VP and activation of p44/42 in the DP.

The p53 protein is a transcription factor that can regulate expression of a variety of target genes (39). As shown in Fig. 3, we observed increased levels of p21 [involved in p53-mediated cell cycle arrest (40)] and PAI-1 [involved in p53-mediated cellular senescence (41)], concomitant with increased steady-state levels of p53 as a function of abrogated IGF-IR expression in DP tissues. This was consistent with the increased levels of SA-βgal previously noted in the DP of IGF-IR knockout mice (Fig. 2). However, reduced levels of PAI-1 expression seemed concomitant with decreased IGF-IR expression in VP despite only very modest changes in the level of p21 protein. Taken together, these data support a differential role for p53-mediated responses in VP and DP epithelium in response to ablated IGF-IR signaling.

Conditional deletion of IGF-IR does not hinder progressive prostate cancer in a p53 depletion-dependent model of multistage tumorigenesis. To investigate the possibility that targeted inhibition of IGF-IR signaling could possibly exacerbate tumor progression in prostate cancer with compromised p53 function, we generated cohorts of 18- and 24-week-old IGF-IR$^{loxP/loxP}$;Cre;TRAMP, IGF-IR$^{loxP/wt}$;Cre;TRAMP, and IGF-IR$^{loxP/loxP;loxP/wt}$;TRAMP mice (24). As shown in Table 2, the incidence of lobe confined and compound lesions were not reduced by titration [IGF-IR$^{loxP/wt}$;Cre;TRAMP] or ablation [IGF-IR$^{loxP/loxP}$;Cre;TRAMP] of IGF-IR at any age. Indeed, at 18 weeks of age, although 38% (n = 8) of IGF-IR titration and 14% (n = 7) of IGF-IR knockout mice had confined or compound lesions, we only observed these lesions in 6% (n = 18) of control mice. Although we did not find a significant difference in the tumor weights between IGF-IR$^{loxP/loxP}$;Cre;TRAMP (1.99 ± 3.47 g and 2.2 ± 2.74 g) and IGF-IR$^{loxP/loxP}$ or IGF-IR$^{loxP/wt}$;TRAMP mice (0.65 ± 0.20 g and 2.36 ± 3.12 g) at 18 or 24 weeks of age, respectively, we did determine a significant increase (1.69 ± 1.57 g; P = 0.02; n = 8) in tumor weights at 18 weeks of age in the IGF-IR$^{loxP/wt}$;Cre;TRAMP mice compared with IGF-IR$^{loxP/loxP}$ or IGF-IR$^{loxP/wt}$;TRAMP mice (0.65 ± 0.20 g; n = 18). Remarkably, 43% and 67% of titration [IGF-IR$^{loxP/wt}$;Cre;TRAMP] and 29% and 71% of knockout [IGF-IR$^{loxP/loxP}$;Cre;TRAMP] mice contained aggressive high-grade poorly differentiated and phylloides-like adenocarcinomas (Fig. 4) compared with 13% and 41% of control [IGF-IR$^{loxP/loxP}$;TRAMP] animals at 18 and 24 weeks of age, respectively (Table 2). We confirmed that prostate tissue–specific recombination at the IGF-IR loci had occurred (Supplementary Fig. S3) and that expression of SV40 Tag was not influenced by loss of IGF-IR in our system (data not shown). Remarkably, all advanced tumors had essentially lost IGF-IR protein expression, irrespective of IGF-IR loci status but consistent with previous reports (Supplementary Fig. S3; ref. 15).

Discussion

Studies in GEM models have generally supported a relationship between IGF-I action and prostate disease. Recently, we reported that enforced expression of IGF-I in prostate epithelium could promote preneoplastic growth but was insufficient to cause carcinoma (18). As well, crossing the *lit* mice with TRAMP (28) showed that although chronically reduced systemic IGF-I and GH expression could significantly delay tumor-related death, the direct role of IGF-I signaling at the level of the prostate epithelium was not specifically addressed nor was the relative contribution of reduced GH levels to prolonged survival.

To more rigorously address the cell autonomous role of IGF-IR in prostate gland biology and cancer, we generated a conditional knockout mouse model and showed that IGF-IR signaling is absolutely required to maintain normal epithelial cell homeostasis. Although substantial evidence predicted that loss of functional IGF-IR expression would lead to prominent cell death, we were surprised to find that abrogation of IGF-IR in the luminal epithelial compartment of DP, LP, and VP lobes consistently correlated with epithelial cell proliferation and a development of focal hyperplasia in young mice. Remarkably, proliferation in DP and LP was found to be concomitant with activation of phosphorylated p44/42, thereby implicating a negative relationship between IGF-IR expression and ERK1/2 activation in these tissues. It was curious that loss of IGF-IR did not seem to directly influence the expression or activation of known positive regulators of ERK1/2 (i.e., Akt, Src, and Raf) or the negative regulators PP2A and MKP3. Efforts are currently under way to more comprehensively study the molecular mechanism whereby loss of IGF-IR expression positively influences ERK1/2 activation and whether this represents a direct or indirect relationship.

Although the loss of IGF-IR in young mice was strongly correlated with proliferation, the hyperplastic lesions did not seem to progress with age. Indeed, we observed a strong correlation with increased cellular senescence in the older cohorts. Because sustained activation of Ras-MAPK signaling is able to promote oncogene-induced cellular senescence (42, 43), it is tempting to speculate that IGF-IR suppresses cellular senescence via the inhibition of phosphorylated p44/42 accumulation and activity, although additional mechanisms may be involved.

It should be noted that tissue-specific ablation in the IGF-IR$^{loxP/wt}$;Cre or IGF-IR$^{loxP/loxP}$;Cre mice could not have influenced overall GH or IGF signaling compared with the controls. Indeed, any significant increase (or decrease) in secretion of systemic GHRH, GH, or IGF-I during the growth period of the animal would have resulted in a significant change in overall body size, and the data presented in Table 1 clearly show that animal body size was similar in all three groups at 12 and 24 months. Moreover, no significant alterations in the size of adipose tissue deposits were noted in the adults and no alterations in genitourinary or prostate wet weights were found to support a possible influence of any increased local IGF-I production on the microenvironment.

The implications of our study are 2-fold. First, our data suggest that IGF-IR activity may relate to the incidence of prostate cancer by suppressing cellular senescence and apoptosis to allow epithelial cells to survive spontaneous transformation while enforcing a strong differentiation block. Second, our data indicate that any decrease in circulating IGF-I in combination with changes to p53 that would physiologically accompany normal aging would provide selective advantage to transformed epithelial cells that could overcome the IGF-IR–mediated differentiation block and progress toward more invasive and disseminated forms of carcinoma. We have previously proposed the hurdle hypothesis to explain how factors that contribute to the height of the differentiation "hurdle" in essence will determine how aggressive a cancer must become to overcome the differentiation barrier/blockade to achieve malignant transformation (18). Because abrogation of functional IGF-IR expression actually promoted earlier emergence of more aggressive, less-differentiated carcinomas in a p53-compromised model of prostate cancer, the current data support the hypothesis that titration of IGF-IR signaling reduces the prodifferentiation block. Importantly, these findings are in remarkable agreement with a prospective study showing a strong association between

lower-grade (Gleason score <7) clinical prostate cancer and elevated serum IGF-I levels (44) and an elevated ratio of IGF-I to IGFBP-3 and the risk of developing extraprostatic and distant metastasis (44, 45).

In summary, GEM models are helping us to define a new paradigm for IGF-I action in the prostate gland that should further help guide translational initiatives to target the IGF-I axis in prostate and other cancers using small-molecule inhibitors and other therapeutic strategies (46). Although we have focused on the enforced expression of IGF-I or abrogation of IGF-IR directly in the prostate, it should be very interesting to determine the effect on tumor initiation and progression in GEM models using the conditional liver-specific IGF-I knockout model (47) that reduces circulating IGF-I without concomitant decrease in GH. As well, it will be interesting to further elucidate the role of p53 and aging on the incidence and nature of prostate cancer.

Acknowledgments

Received 12/5/2007; revised 2/13/2008; accepted 2/25/2008.

Grant support: National Cancer Institute grants CA82807 (N.M. Greenberg) and CA84296 (F. Wang and N.M. Greenberg), Prostate Cancer Foundation (P.J. Kaplan-Lefko and N.M. Greenberg), and Phi Beta Psi (N.M. Greenberg).

The costs of publication of this article were defrayed in part by the payment of page charges. This article must therefore be hereby marked *advertisement* in accordance with 18 U.S.C. Section 1734 solely to indicate this fact.

We thank Deborah Kwok, Susanna Hernandez, and Claire Gibson for technical support and Krisitine Griffith for administrative support.

References

1. Baserga R, Peruzzi F, Reiss K. The IGF-1 receptor in cancer biology. Int J Cancer 2003;107:873–7.
2. Jones JI, Clemmons DR. Insulin-like growth factors and their binding proteins: biological actions. Endocr Rev 1995;16:3–34.
3. De Meyts P, Palsgaard J, Sajid W, Theede AM, Aladdin H. Structural biology of insulin and IGF-1 receptors. Novartis Found Symp 2004;262:160–71; discussion 71–6, 265–8.
4. Holly J. Physiology of the IGF system. Novartis Found Symp 2004;262:19–26; discussion 26–35, 265–8.
5. Rosenzweig SA. What's new in the IGF-binding proteins? Growth Horm IGF Res 2004;14:329–36.
6. Fang P, Hwa V, Rosenfeld R. IGFBPs and cancer. Novartis Found Symp 2004;262:215–30; discussion 30–4, 65–8.
7. Morrione A, Valentinis B, Li S, Ooi JY, Margolis B, Baserga R. Grb10: a new substrate of the insulin-like growth factor I receptor. Cancer Res 1996;56:3165–7.
8. Myers MG, Jr., Grammer TC, Wang LM, et al. Insulin receptor substrate-1 mediates phosphatidylinositol 3′-kinase and p70S6k signaling during insulin, insulin-like growth factor-1, and interleukin-4 stimulation. J Biol Chem 1994;269:28783–9.
9. LeRoith D, Werner H, Beitner-Johnson D, Roberts CT, Jr. Molecular and cellular aspects of the insulin-like growth factor I receptor. Endocr Rev 1995;16:143–63.
10. Pollak MN, Schernhammer ES, Hankinson SE. Insulin-like growth factors and neoplasia. Nat Rev Cancer 2004;4:505–18.
11. Cohen P, Graves HC, Peehl DM, Kamarei M, Giudice LC, Rosenfeld RG. Prostate-specific antigen (PSA) is an insulin-like growth factor binding protein-3 protease found in seminal plasma. J Clin Endocrinol Metab 1992; 75:1046–53.
12. Kaleko M, Rutter WJ, Miller AD. Overexpression of the human insulinlike growth factor I receptor promotes ligand-dependent neoplastic transformation. Mol Cell Biol 1990;10:464–73.
13. LeRoith D, Roberts CT, Jr. The insulin-like growth factor system and cancer. Cancer Lett 2003;195:127–37.
14. Tennant MK, Thrasher JB, Twomey PA, Birnbaum RS, Plymate SR. Insulin-like growth factor-binding proteins (IGFBP)-4, -5, and -6 in the benign and malignant human prostate: IGFBP-5 messenger ribonucleic acid localization differs from IGFBP-5 protein localization. J Clin Endocrinol Metab 1996;81:3783–92.
15. Kaplan PJ, Mohan S, Cohen P, Foster BA, Greenberg NM. The insulin-like growth factor axis and prostate cancer: lessons from the transgenic adenocarcinoma of mouse prostate (TRAMP) model. Cancer Res 1999;59: 2203–9.
16. Ahlen J, Wejde J, Brosjo O, et al. Insulin-like growth factor type 1 receptor expression correlates to good prognosis in highly malignant soft tissue sarcoma. Clin Cancer Res 2005;11:206–16.
17. Ma Z, Gibson SL, Byrne MA, Zhang J, White MF, Shaw LM. Suppression of insulin receptor substrate 1 (IRS-1) promotes mammary tumor metastasis. Mol Cell Biol 2006;26:9338–51.
18. Kaplan-Lefko PJ, Sutherland BW, Evangelou AI, et al. Enforced epithelial expression of IGF-1 causes hyperplastic prostate growth while negative selection is requisite for spontaneous metastogenesis. Oncogene 2007 [Epub ahead of print].
19. DiGiovanni J, Bol DK, Wilker E, et al. Constitutive expression of insulin-like growth factor-1 in epidermal basal cells of transgenic mice leads to spontaneous tumor promotion. Cancer Res 2000;60:1561–70.
20. DiGiovanni J, Kiguchi K, Frijhoff A, et al. Deregulated expression of insulin-like growth factor 1 in prostate epithelium leads to neoplasia in transgenic mice. Proc Natl Acad Sci U S A 2000;97:3455–60.
21. Colao A, Marzullo P, Spiezia S, et al. Effect of growth hormone (GH) and insulin-like growth factor I on prostate diseases: an ultrasonographic and endocrine study in acromegaly, GH deficiency, and healthy subjects. J Clin Endocrinol Metab 1999;84:1986–91.
22. Wennbo H, Gebre-Medhin M, Gritli-Linde A, Ohlsson C, Isaksson OG, Tornell J. Activation of the prolactin receptor but not the growth hormone receptor is important for induction of mammary tumors in transgenic mice. J Clin Invest 1997;100:2744–51.
23. Wennbo H, Kindblom J, Isaksson OG, Tornell J. Transgenic mice overexpressing the prolactin gene develop dramatic enlargement of the prostate gland. Endocrinology 1997;138:4410–5.
24. Greenberg NM, DeMayo F, Finegold MJ, et al. Prostate cancer in a transgenic mouse. Proc Natl Acad Sci U S A 1995;92:3439–43.
25. Kanety H, Madjar Y, Dagan Y, et al. Serum insulin-like growth factor-binding protein-2 (IGFBP-2) is increased and IGFBP-3 is decreased in patients with prostate cancer: correlation with serum prostate-specific antigen. J Clin Endocrinol Metab 1993;77:229–33.
26. Shariat SF, Gottenger E, Nguyen C, et al. Preoperative blood reverse transcriptase-PCR assays for prostate-specific antigen and human glandular kallikrein for prediction of prostate cancer progression after radical prostatectomy. Cancer Res 2002;62:5974–9.
27. Jansson JO, Downs TR, Beamer WG, Frohman LA. Receptor-associated resistance to growth hormone-releasing factor in dwarf "little" mice. Science 1986; 232:511–2.
28. Majeed N, Blouin MJ, Kaplan-Lefko PJ, et al. A germ line mutation that delays prostate cancer progression and prolongs survival in a murine prostate cancer model. Oncogene 2005;24:4736–40.
29. Sell C, Dumenil G, Deveaud C, et al. Effect of a null mutation of the insulin-like growth factor I receptor gene on growth and transformation of mouse embryo fibroblasts. Mol Cell Biol 1994;14:3604–12.
30. Jin C, McKeehan K, Guo W, et al. Cooperation between ectopic FGFR1 and depression of FGFR2 in induction of prostatic intraepithelial neoplasia in the mouse prostate. Cancer Res 2003;63:8784–90.
31. Holzenberger M, Hamard G, Zaoui R, et al. Experimental IGF-I receptor deficiency generates a sexually dimorphic pattern of organ-specific growth deficits in mice, affecting fat tissue in particular. Endocrinology 2001;142:4469–78.
32. Delmas V, Martinozzi S, Bourgeois Y, Holzenberger M, Larue L. Cre-mediated recombination in the skin melanocyte lineage. Genesis 2003;36:73–80.
33. Shappell SB, Thomas GV, Roberts RL, et al. Prostate pathology of genetically engineered mice: definitions and classification. The consensus report from the Bar Harbor meeting of the Mouse Models of Human Cancer Consortium Prostate Pathology Committee. Cancer Res 2004;64:2270–305.
34. Johnson MA, Hernandez I, Wei Y, Greenberg N. Isolation and characterization of mouse probasin: an androgen-regulated protein specifically expressed in the differentiated prostate. Prostate 2000;43:255–62.
35. Wu X, Wu J, Huang J, et al. Generation of a prostate epithelial cell-specific Cre transgenic mouse model for tissue-specific gene ablation. Mech Dev 2001;101:61–9.
36. Jin C, McKeehan K, Wang F. Transgenic mouse with high Cre recombinase activity in all prostate lobes, seminal vesicle, and ductus deferens. Prostate 2003;57: 160–4.
37. Lowe SW, Cepero E, Evan G. Intrinsic tumour suppression. Nature 2004;432:307–15.
38. Feng Z, Hu W, Teresky AK, Hernando E, Cordon-Cardo C, Levine AJ. Declining p53 function in the aging process: a possible mechanism for the increased tumor incidence in older populations. Proc Natl Acad Sci U S A 2007;104:16633–8.
39. Levine AJ. p53, the cellular gatekeeper for growth and division. Cell 1997;88:323–31.
40. Chang BD, Swift ME, Shen M, Fang J, Broude EV, Roninson IB. Molecular determinants of terminal growth arrest induced in tumor cells by a chemotherapeutic agent. Proc Natl Acad Sci U S A 2002;99:389–94.
41. Kortlever RM, Higgins PJ, Bernards R. Plasminogen activator inhibitor-1 is a critical downstream target of p53 in the induction of replicative senescence. Nat Cell Biol 2006;8:877–84.
42. Collado M, Serrano M. The senescent side of tumor suppression. Cell Cycle 2005;4:1722–4.
43. Braig M, Schmitt CA. Oncogene-induced senescence: putting the brakes on tumor development. Cancer Res 2006;66:2881–4.
44. Chan JM, Stampfer MJ, Ma J, et al. Insulin-like growth factor-I (IGF-I) and IGF binding protein-3 as predictors of advanced-stage prostate cancer. J Natl Cancer Inst 2002;94:1099–106.
45. Chan JM, Stampfer MJ, Giovannucci E, et al. Plasma insulin-like growth factor-I and prostate cancer risk: a prospective study. Science 1998;279:563–6.
46. Garber K. IGF-1: old growth factor shines as new drug target. J Natl Cancer Inst 2005;97:790–2.
47. Liu JL, Yakar S, LeRoith D. Conditional knockout of mouse insulin-like growth factor-1 gene using the Cre/loxP system. Proc Soc Exp Biol Med 2000;223:344–51.